Original Research

SPINE RESEARCH

OPEN

miR-146a-5p induces intervertebral disc degeneration by targeting SOD2

Chu Gao[a,b], Dong Wang[b], Chuxin Zhou[b], Jianxin Mao[b], Zhuojing Luo[a,b], Liu Yang[a,b], Di Wang[b]*

Abstract

Objectives: This study aimed to investigate the role and underlying mechanism of miR-146a-5p in inflammation-induced intervertebral disc degeneration (IDD).

Methods: We performed miRNA sequencing and bioinformatic analysis on IL-1β-treated rat primary nucleus pulposus cells (RPNPCs). The function of miR-146a-5p was validated using mimics and inhibitors in vitro, and its therapeutic effect was assessed in a needle-punctured rat disc organotypic explant model. Target gene prediction and validation, along with loss- and gain-of-function experiments for Sod2, were conducted.

Results: miR-146a-5p was significantly upregulated in degenerative human discs and IL-1β-treated RPNPCs. Its overexpression promoted extracellular matrix catabolism and inhibited anabolism, and induced apoptosis in RPNPCs, while its inhibition exerted protective effects. Mechanistically, miR-146a-5p directly targeted and downregulated superoxide dismutase 2 (SOD2). Knockdown of *Sod2* exacerbated degenerative phenotypes, whereas its overexpression mitigated IL-1β-induced damage. In the explant model, inhibition of miR-146a-5p restored *Sod2* expression and ameliorated disc degeneration.

Conclusions: miR-146a-5p drives inflammation-induced IDD by suppressing *Sod2*, leading to mitochondrial oxidative stress and NP cell dysfunction. Targeting the miR-146a-5p/Sod2 axis represents a novel potential therapeutic strategy for IDD.

Keywords: IL-1β, intervertebral disc degeneration, miR-146a-5p, miRNA, *Sod2*

1. Introduction

Low back pain is a common musculoskeletal disease and a leading cause of disability, which occurs in almost everyone during their lifetime.[1–4] To date, numerous studies have confirmed a causative link between low back pain and intervertebral disc degeneration (IDD).[5–7] With population aging, the incidence and disability burden attributable to IDD are rising dramatically, severely impacting patients' quality of life and work capacity.[8,9]

The intervertebral disc (IVD) consists of a central nucleus pulposus (NP), the peripheral annulus fibrosus (AF), and the covering cartilage endplates. As the central part of IVDs, NP tissues function as a cushioning pad between adjacent vertebrates, maintaining the stability and flexibility of the spine at the same time.[10,11] The NP tissue, which secretes proteoglycans and type II collagen, is crucial for regulating the extracellular matrix (ECM) abundance and, consequently, the water content and disc height. The degeneration of the NP is considered a significant pathological progression in IDD.[11,12] To date, various factors have been reported to engage in the occurrence and development of IDD, including genetics, aging, and even daily actions, such as smoking, excessive loading, and even circadian disturbance. Although the precise pathogenesis of IDD remains elusive, inflammation is generally thought to be the most common cause of IDD.[12–14] Moreover, as the degeneration of IVDs aggravates, NP cells secrete more inflammatory mediators, such as interleukin (IL)-1 and tumor necrosis factor alpha (TNF-α), resulting in the secretion of matrix-degrading enzymes and thus leading to the degradation of ECM, and finally contributing to the progression of IDD.[15–17] However, the mechanism of inflammation-induced IDD has not been fully elucidated.

miRNA is a class of endogenous noncoding RNA, which widely exists in eukaryotic cells and plays an important role in cell differentiation, proliferation, and survival. miRNA

CG and DW contributed to this article equally.

Supplemental Digital Content is available for this article.

[a] Institute of Medical Research, Northwestern Polytechnical University, Xi'an, China, [b] Institute of Orthopedic Surgery, Xijing Hospital, Fourth Military Medical University, Xi'an, China.

* Correspondence: Di Wang, Institute of Orthopedic Surgery, Xijing Hospital, Fourth Military Medical University, No. 169, Changle West Road, Xincheng District, Xi'an, Shaanxi Province, China (e-mail: dr.wangdi@qq.com).

Spine Research (2025) 1:2;65–77

Received: 18 July 2025 / Accepted: 30 July 2025

http://dx.doi.org/10.1097/br9.0000000000000011

regulates the transcription and translation of mRNA by targeting its 3′-untranslated region (3′-UTR), thus resulting in mRNA translational inhibition or degradation.[18] Previous studies have confirmed that miRNAs are involved in the pathological processes of IDD, such as miR-141, miR-338-3p, miR-22-3p and hsa-let-7f-1-3p, which offer some potential therapeutic targets.[19–23] In addition, some essential functional regulatory genes, such as *Sirt1*, *Sirt6*, and *Bmal1*, have also been proved as the inhibitory targets of these miRNAs.[20,21,23–25] However, it is still unclear which miRNA plays the most important role in the process of inflammation-induced IDD and which gene is subsequently inhibited by this miRNA. In this study, a miRNA sequencing strategy was applied to identify differentially expressed miRNAs in rat primary nucleus pulposus cells (RPNPC) treated with IL-1 or not, and we found that the expression of miR-146a-5p was significantly increased in IL-1β-treated RPNPC. Mechanically, *Sod2,* a gene encoding superoxide dismutase (SOD2), a matrix enzyme expressed in mitochondria and known as an important free radical scavenger, was the target gene of miR-146a-5p. Overexpression of miR-146a-5p by mimics decreased the expression of SOD2 and increased the inflammatory response, oxidative stress, and apoptosis of RPNPC, while inhibition of miR-146a-5p by its inhibitor significantly ameliorated IL-1β-induced IDD phenotypes. This study provides a new understanding of the role of miRNAs in inflammation-induced IDD and puts forward a potential therapeutic target for the prevention and treatment of IDD.

2. Materials and methods

2.1. Patient samples

NP specimens were obtained from 12 patients (5 males and 7 females; mean age = 49.9 ± 14.4 years) with degenerative disc disease or scoliosis. The degree of IDD was assessed by 3 other blinded orthopedic researchers according to the modified Pfirrmann grading system by magnetic resonance imaging. Grade II (n = 3) and III (n = 3) samples were combined into a moderate group (mean age = 44.7 ± 15.2), while Grade IV (n = 3) and V (n = 3) samples were combined into a severe group (mean age = 55.2 ± 12.6 years). All the information of these samples is shown in Table S1, Supplemental Digital Content, https://links.lww.com/SPRES/A3. Ethics approval was obtained from the Institutional Review Board of Xijing Hospital of Fourth Military Medical University (KY20203146-1), and informed consent was obtained from each donor. The work presented in this article was performed according to The Code of Ethics of the World Medical Association (Declaration of Helsinki).

2.2. Isolation, culture, and in vitro IDD model of rat primary NP cells

In this study, RPNPC were isolated from male Sprague-Dawley (SD) rats (8 weeks). Rats were euthanized by inhaling excessive isoflurane. Under aseptic conditions, the rat tail was taken, the tail vein was separated, and the gel-like NP tissue was isolated from the AF under a microscope. For the isolation of RPNPC, the obtained NP tissue was digested in 0.4% pronase (10165921001, Roche Diagnostics, Germany) and 0.0125% collagenase P for 30 minutes (11213865001, Roche Diagnostics, Germany), and then the digested tissue was washed 3 times with phosphate buffer through a cell filter with a pore diameter of 100 μm. The isolated cells were stored in DF12 medium containing 10% fetal bovine serum (10099141C, Gibco), supplemented with 1% penicillin-streptomycin combination (15070063, Gibco), and cultured in 5% carbon dioxide incubator. The primary cells used in this study are the second generation. *In vitro* inflammation model, IL-1β (10 ng/24 h) was used to treat the second generation of primary cells.[15,26,27]

2.3. miRNA sequencing

GENE DENOVO tested the quality and amount of miRNA and constructed and sequenced the miRNA library. Total RNA was extracted from the samples by the TRIzol method, and the bands in the range of 18–30 nt were selected by polyacrylamide gel electrophoresis (PAGE), and small RNA was recovered. The 3' and 5' connectors were connected, respectively, and then the small RNA connected to the 2 connectors was reverse transcribed and polymerase chain reaction (PCR) amplified. Finally, the PAGE gel was used to recover and purify the 140 bp bands, dissolve in EB solution, and complete the library construction. The constructed library uses Agilent2100 and ABI Step One Plus Real-Time PCR System (Life Technologies) to detect the quality and yield, and is sequenced on the computer. The information analysis part is mainly divided into 3 modules. First of all, the original sequencing data of each sample are processed to get the tag sequence of the small RNA. Secondly, the tag was annotated, the tag sequence composition of the small RNA in the sample was identified, and the miRNA was identified. Finally, the miRNA expression profile was obtained, and miRNA gene difference analysis, target gene prediction, and target gene enrichment analysis were obtained.

2.4. Organotypic tissue-explant of IVD

Under the approval of the Animal Experiment Administration Committee of the Air Force Military Medical University, tails were collected from 10.8-week SD rats under pathogen-free conditions, after they were euthanized. The muscles and tendons were dissected and removed by a scalpel and surgical scissors under aseptic conditions. Explants consist of the IVD and 2 adjacent vertebrae. The explants were randomly divided into 4 groups: uninjured group (Control), injured group (Needle-punctured), injured and mimics-treated group (Needle-punctured + mimics), and injured and inhibitor-treated group (Needle-punctured + inhibitor). AF was stabbed with a 20 G needle to enter the center of the NP, rotates 360 degrees, and stays for 1 minute. The explants were cultured in DF12 containing 10% fetal bovine serum (#10099141C, Gibco), supplemented with 1%

penicillin-streptomycin combination (#15070063, Gibco) at 37 °C in a humidified atmosphere of 5% CO_2. The medium was replaced with fresh medium every other day. After 14 days, the explants of all groups were collected. No explant was excluded from the analysis.[15]

2.5. In vitro siRNA, miRNA, and adenovirus transfection

Mimics and inhibitors targeting rat miR-146a-5p were designed and synthesized by Tsingke (Beijing, China) *in vitro*. The mimics and inhibitor sequences used in this study are listed in Table 2, Supplemental Digital Content, https://links.lww.com/SPRES/A3. The siRNA double strand for rat *Sod2* was designed and synthesized by Hanbio (China). The siRNA sequences used in this study are listed in Table 2, Supplemental Digital Content, https://links.lww.com/SPRES/A3. According to the manufacturer's instructions, RNAfit reagent (Hanbio, China) was used for siRNA transfection. To put it simply, the RPNPC of the second passage were seeded in a 6-well plate. After adhesion, the cells were incubated with Optic-MEM medium (# 31985062 Thermo, USA) at 37 °C for 2 hours. Then, 100 nM siRNA or NC siRNA was transfected with RNAfit and incubated at 37 °C for 6 hours. Finally, the cells were washed with phosphate-buffered saline (PBS) and replaced with complete medium. After 24 hours, the cells were treated accordingly. For the overexpression of *Sod2*, an adenovirus vector overexpressing rat *Sod2* was manufactured by Hanbio, and the transfection was performed according to the manufacturer's instructions.

2.6. Protein extraction and western blotting analysis

RPNPC were washed with PBS (Gibco) twice. Then the cells were lysed in radioimmune precipitation assay buffer (Beyotime, China) with a complete protease inhibitor cocktail (Roche, Germany). The total protein of RPNPC was collected by centrifuging at 12,500 rpm for 15 minutes at 4 °C. The concentrations of protein were measured using the Pierce BCA Protein Assay Kit (Thermo Fisher Scientific, USA). The total proteins were diluted by loading buffer, heated at 95 °C for 5 minutes, and then certain amounts of protein were separated in 10% sodium dodecyl sulfate polyacrylamide gels (SDS-PAGE) and transferred to nitrocellulose membranes (Millipore, Germany). Then the nitrocellulose membranes were blocked by 5% skim milk in Tris-buffered saline containing 0.1% Tween 20 for 40 minutes at room temperature. These membranes were incubated overnight at 4 °C with primary antibodies, including the following: anti-SOD2 (1:1000), anti-Aggrecan (1:1000), anti-matrix metalloproteinase 3 (MMP3) (1:1000), and anti-glyceraldehyde 3-phosphate dehydrogenase (GAPDH) (1:2000). Then the membranes were incubated with the horseradish peroxidase-linked goat antirabbit IgG or horse antimouse IgG secondary antibody for 1 hour at room temperature. The nitrocellulose membranes were washed 3 times with tris-buffered saline containing 0.1% Tween 20 for 15 minutes after each step. Finally, the nitrocellulose membranes were visualized by Immobilon Western Chemiluminescent horseradish peroxidase Substrate (Millipore Corporation, Germany, #WBKLS0100), and the density of nitrocellulose membranes was quantified by Image J software (National Institutes of Health, Bethesda, MD, USA).[15,26] The detailed information of antibodies used in this study is listed in Table 3, Supplemental Digital Content, https://links.lww.com/SPRES/A3.

2.7.RNA extraction and quantitative reverse transcription-polymerase chain reaction analysis

Total RNA of RPNPC, human NP tissues, or rat coccygeal NP tissues was harvested using Mini BEST Universal RNA Extraction Kit (TaKaRa, China) according to the manufacturer's instructions. Reverse transcription was performed with Prime Script RT Master Mix (TaKaRa, China). Synthesized cDNA was then subjected to qPCR analysis using TB Green Premix Ex Taq II (TaKaRa, China). The reactions were performed with CFX96 (Bio-Rad, USA). Gene expression levels were reported as relative fold change, with *Gapdh* (*Acan*, *Mmp3*, *Sod2*) and *U6* (miR-146a-5p) as an internal control. Primers sequences used in this study are shown in Table 4, Supplemental Digital Content, https://links.lww.com/SPRES/A3.

2.8. Apoptosis assay

For *in vitro* cell experiments, RPNPC were harvested in 0.25% trypsin and washed 3 times with cold PBS. The apoptosis of RPNPC was evaluated by Annexin V-PE/propidium iodide (PI) apoptosis detection kit (BD Biosciences, USA) by flow cytometry. For disc sections, terminal deoxynucleotidyl transferase dUTP nick end labeling assay was performed using *In Situ* Cell Death Detection Kit (#11684795910, Roche Diagnostics, Germany) according to manufacturer's instructions.[26,28]

2.9. In vitro immunofluorescence staining

RPNPC were fixed in freshly prepared 4% paraformaldehyde for 30 minutes, permeabilized by 0.1% Triton X-100 (Beyotime, China) for 30 minutes. Then the cells were blocked by 1% BSA in PBS for 1 hour, incubated with primary antibody at 4 °C overnight, with appropriate secondary antibodies at room temperature (RT) for 2 hours, and with 4',6-diamidino-2-phenylindole (C1006, Beyotime, China) at RT for 10 minutes. Finally, the cells were analyzed under a fluorescence microscope (BX53, OLYMPUS, Japan).[29,30] The antibodies used for *in vitro* immunofluorescence (IF) staining are listed in Table 3, Supplemental Digital Content, https://links.lww.com/SPRES/A3.

2.10. Histology and IF staining for disc sections

Explants were fixed in 4% freshly prepared paraformaldehyde for 48 hours, decalcified for 8 weeks with 10% ethylenediaminetetraacetic acid at RT under gentle shaking, then dehydrated, paraffin-embedded, and sectioned at 5 μm. The sections were deparaffinized by xylene and rehydrated by ethanol. The hematoxylin-eosin (HE) staining

kit (Solarbio, China) or safranin O-fast green staining kit (Solarbio, China) was used according to the manufactures' instructions, and the sections were graded by a previously published method. For the IF staining, citrate buffer (0.1 mol/L, pH 6.0) was used to perform antigen-retrieval on deparaffinized and dehydrated sections. After blocking in 10% normal goat serum (Solarbio, China) at RT for 1 hour, the sections were then incubated with primary antibody at 4 °C overnight, with appropriate secondary antibodies at RT for 2 hours and with 4',6-diamidino-2-phenylindole (C1006, Beyotime, China) for 10 minutes. Finally, the sections were analyzed under a fluorescence microscope (BX53, OLYMPUS, Japan). Fluorescence intensity was quantified using ImageJ (National Institutes of Health, USA) software.[30] The antibodies used for sections' IF staining in the study are listed in Table 3, Supplemental Digital Content, https://links.lww.com/SPRES/A3.

2.11. Statistical analysis

Data are presented as mean ± SD in all experiments. Whether the data present a normal distribution was tested by the Shapiro–Wilk test or D'Agostino test. The differences between 2 or multiple groups were analyzed by Student *t* test or one-way analysis of variance, followed by Tukey multiple-comparison post hoc test, respectively. All statistical analyses were performed with SPSS 22.0 and GraphPad Prism 9.0 software. Differences were considered statistically significant at p value < 0.05.

3. Results

3.1. The expression of miR-146a-5p was significantly upregulated during IDD

Given the central role of inflammation in IDD pathogenesis and the established regulatory functions of miRNAs in IVD homeostasis, we first comprehensively profiled miRNA expression in RPNPCs under inflammatory conditions. The RPNPC were subjected to IL-1β (10 ng/mL) for 24 hours to simulate an inflammatory microenvironment and then harvested, and the miRNA sequencing was carried out by GENE DENOVO. Compared with untreated controls, the IL-1β-treated group exhibited 297 upregulated and 198 downregulated miRNAs, and some significantly expressed candidate miRNAs were shown in the heat map (Fig. 1A). Gene ontology (GO) and Kyoto Encyclopedia of Genes and Genomes (KEGG) enrichment analysis were performed based on these differentially expressed miRNAs. The biological process and molecular function of all differentially expressed miRNAs, whether upregulated miRNAs or downregulated miRNAs, focused on the metabolic process and catalytic activity, indicating a coherent function of these miRNAs (Fig. 1B–E). Among these differentially expressed miRNAs, miR-146a-5p demonstrated the most consistent and pronounced upregulation and was therefore selected for further investigation (Fig. 1F,G). These findings identified miR-146a-5p as a potentially key disease-associated miRNA in IDD.

3.2. Overexpression of miR-146a-5p led to development of degenerative phenotype and apoptosis of RPNPC in vitro, and miR-146a-5p inhibition showed a therapeutic effect against treatment of IL-1β

To ascertain the role of miR-146a-5p during inflammation-induced IDD, overexpression of mimics or inhibition of miR-146a-5p was performed in cultured RPNPCs with or without IL-1β treatment. The aggrecan (ACAN) and catabolism (MMP3) of ECM were evaluated by immunofluorescence staining, quantitative reverse transcription-polymerase chain reaction (qRT-PCR) and western blot. The increased expression of MMP13 and reduced expression of Aggrecan were observed in the IL-1β-treated group, indicating a successful establishment of inflammation-induced IDD model. Similarly, the degradation of ECM was also seen in the miR-146a-5p mimics-treated group, indicating a deleterious effect of miR-146a-5p. On the contrary, the inhibitor of miR-146a-5p slightly promoted the anabolism and inhibited the catabolism of ECM, indicating a protective effect (Fig. 2A–M). Given the established link between IDD progression and NP cell apoptosis. We also evaluated the apoptosis of RPNPC in these groups by Annexin V-PE/PI detection. The results of flow cytometry showed that both IL-1β treatment and miR-146a-5p mimics significantly promoted the apoptosis of RPNPC, and the miR-146a-5p inhibitors partially rescued the apoptosis of RPNPC induced by IL-1β treatment (Fig. 2N,O). Collectively, these results demonstrated that miR-146a-5p critically drives IDD pathogenesis, and its inhibition mitigated inflammation-induced degenerative phenotypes in NP cells.

3.3. miR-146a-5p promoted the development of IDD by targeting Sod2

miRNAs primarily exert their biological functions by inhibiting target gene transcripts. To investigate miR-146a-5p's role in IDD pathogenesis, bioinformatic analysis was performed to predict the downstream target genes of miR-146a-5p. To this end, public databases like RNAhybrid, miRanda, and TargetScan were included in our analysis. GO and KEGG enrichment analysis was performed based on downregulated genes caused by miR-146a-5p. The bubble diagram of KEGG enrichment analysis showed that most of the miR-146a-5p target genes concentrate upon the metabolic pathways, proteoglycan synthesis, cholesterol and glycerolipid metabolism, oxidative phosphorylation, and other metabolic pathways. And the bar diagram of GO enrichment analysis showed metabolism process, biological regulation, and response to stimulus as the top catalogues of biological process (Fig. 3A,B). Coincident portion of the Venn analysis identified *Sod2* as a consensus target (Fig. 3C). 3′-UTR sequence of *Sod2* also showed a binding site of miR-146a-5p according to the public databases (Fig. 3D). In addition, increased miR-146a-5p expression as well as decreased *Sod2* expression were confirmed in human pfirrmann IV-V IVDs compared with the pfirrmann II-III IVDs, further confirming the involvement of

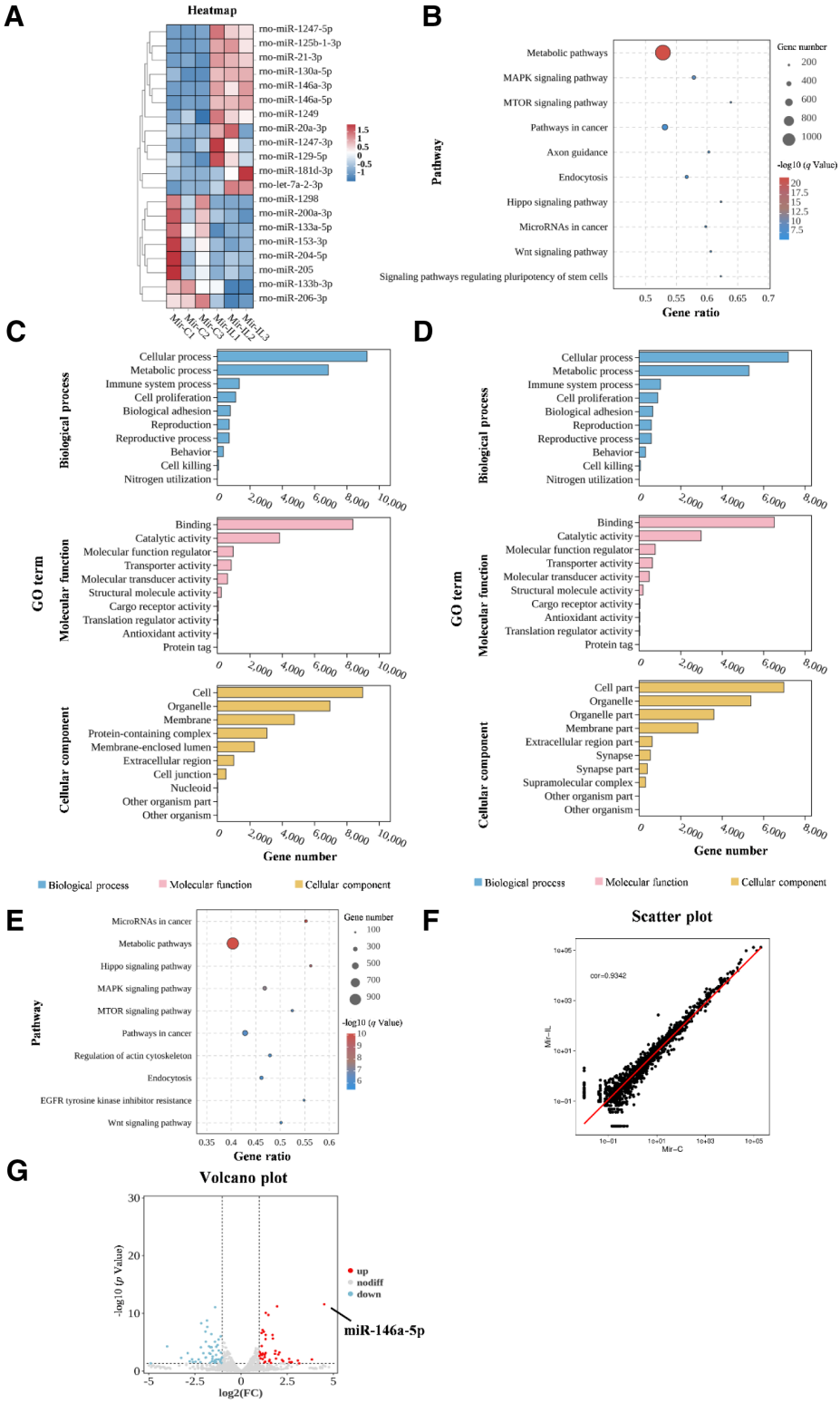

Figure 1. The expression of miR-146a-5p was significantly unregulated under the *in vitro* IDD model. (A) Heatmap of hierarchical clustering with dendrogram showing significantly upregulated (red) and downregulated (blue) genes from miRNA sequencing of rat primary nucleus pulposus cells. Comparison between the control group (Con) and the IL-1β-treated group. (B–C) Enrichment analysis of differentially upregulated genes from miRNA sequencing: (B) KEGG pathways, (C) GO terms. (D–E) Enrichment analysis of differentially downregulated genes from miRNA sequencing: (D) GO terms, (E) KEGG pathways. (F) Scatter plot of miRNA sequencing results depicting global gene expression distribution. (G) Volcano plot of differentially expressed miRNAs. miR-146a-5p is specially labeled, demonstrating significant upregulation ($|\log_2 FC| > 1.5$, $p < 0.001$). Results were shown as mean ± S.D.; $n = 3$; *** $p < 0.005$. GO = Gene Ontology; IL-1β = interleukin-1 beta; KEGG = Kyoto Encyclopedia of Genes and Genomes; S.D. = standard deviation.

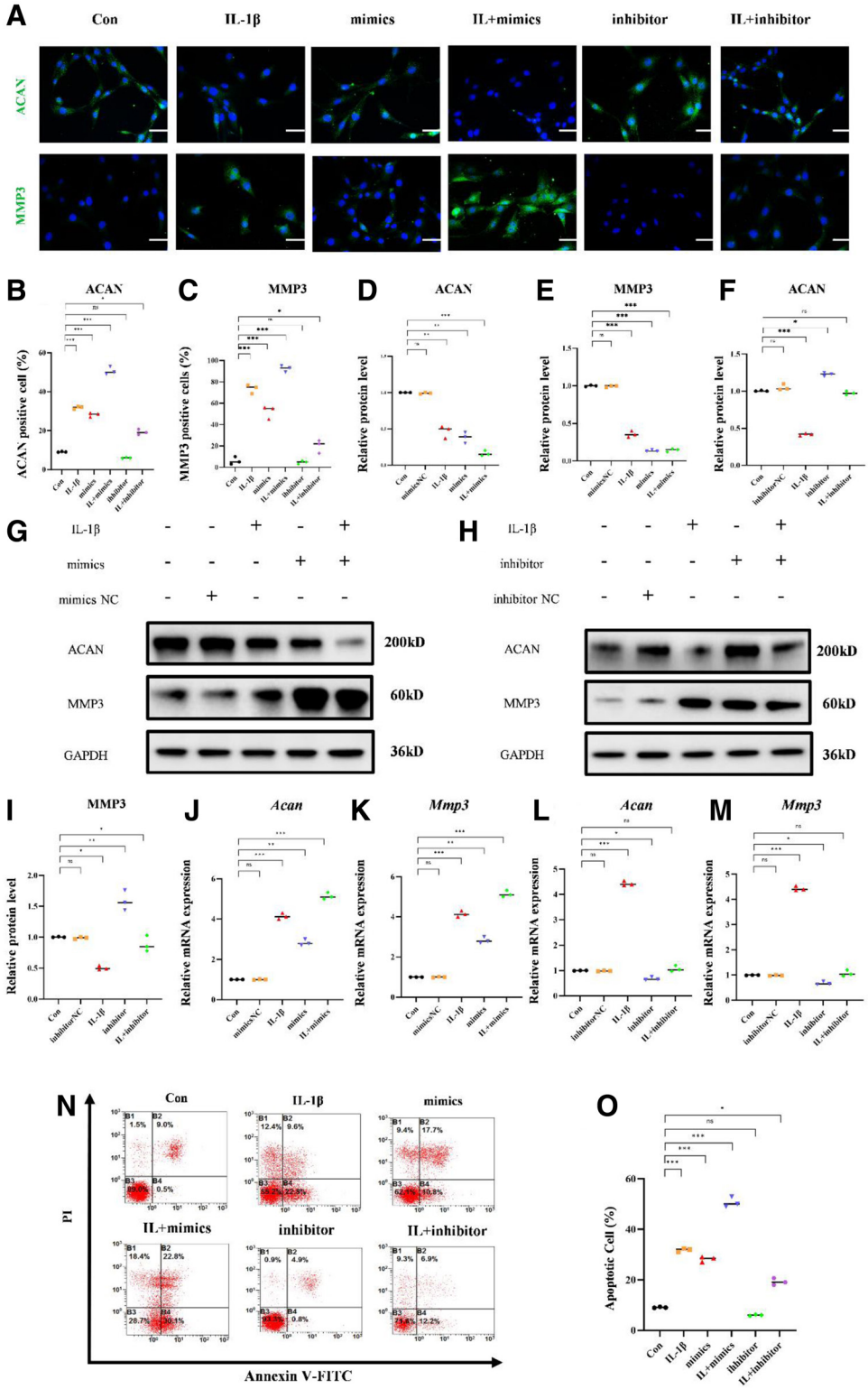

Figure 2. Overexpression of miR-146a-5p led to development of degenerative phenotype and apoptosis of RPNPCs *in vitro*, and miR-146a-5p inhibition showed a therapeutic effect against IL-1β. (A) Immunofluorescence images of ACAN and MMP3 in the Con group, IL-1β-treated group, mimics group, IL + mimics group (in subsequent groups, IL denotes IL-1β inhibitor group), and IL + inhibitor group. (B) Quantification of ACAN immunofluorescence results. (C) Quantification of MMP13 immunofluorescence results. (D) Quantification of ACAN western blot (WB) results (from Panel G). (E) Quantification of MMP3 WB results (from Panel G). (F) Quantification of ACAN WB results (from Panel H). (G) WB results of ACAN and MMP3 in the Con group, mimics NC group, IL-1β-treated group, mimics group, and IL + mimics group. (H) WB results of ACAN and MMP3 in the Con group, inhibitor NC group, IL-1β-treated group, inhibitor group, and IL + inhibitor group. (I) Quantification of MMP3 WB results (from Panel H). (J) qPCR results of ACAN in the Con group, mimics NC group, IL-1β-treated group, mimics group, and IL + mimics group. (K) qPCR results of MMP3 in the Con group, mimics NC group, IL-1β-treated group, mimics group, and IL + mimics group. (L) qPCR results of ACAN in the Con group, inhibitor NC group, IL-1β-treated group, inhibitor group, and IL + inhibitor group. (M) qPCR results of MMP3 in the Con group, inhibitor NC group, IL-1β-treated group, inhibitor group, *(Continued)*

Fig. 2 Continued. and IL + inhibitor group. (N) Apoptosis flow cytometry results in the Con group, IL-1β-treated group, mimics group, IL + mimics group, inhibitor group, and IL + inhibitor group. (O) Quantification of apoptosis flow cytometry results. Results were shown as mean ± S.D.; $n = 3$; * $p < 0.05$, ** $p < 0.01$; *** $p < .005$; ns: not statistically significant; Scale bar = 50 μm. ACAN = aggrecan; IL-1 β = interleukin-1 beta; MMP3 = matrix metalloproteinase 3; RPNPCs = rat primary nucleus pulposus cells.

miR-146a-5p and its target gene *Sod2* in the development of IDD (Fig. 3E,F). To verify the effect of miR-146a-5p on *Sod2*, overexpression of mimics or inhibition of miR-146a-5p was performed in cultured RPNPCs with or without IL-1β treatment, and the expression level of *Sod2* was evaluated by qRT-PCR, western blot analysis, and immunofluorescence staining. Both mimics treatment and IL-1β treatment significantly inhibited the expression of *Sod2*, while the inhibitor of miR-146a-5p partially recovered the decreased expression of *Sod2* under the inflammatory environment (Fig. 3G–N). Collectively, these results established *Sod2* as a direct functional target of miR-146a-5p in IDD.

3.4. Loss of Sod2 led to a dysfunction of RPNPC, and overexpression of Sod2 protected RPNPC against Inflammatory attack

Building on the finding that miR-146a-5p directly targets *Sod2*, we next investigated whether *Sod2* exerts protective effects against IDD pathogenesis. Loss and gain of function of *Sod2* was achieved by the delivery of siRNA targeting *Sod2* or adenovirus overexpressing *Sod2*, respectively. The knockdown efficiency was validated by western blot analysis, and siRNA1 showed the highest efficiency (Fig. 4A,B). The immunofluorescence staining results showed a decreased ACAN and increased catabolism (MMP3) of ECM after the treatment of si*Sod2* (Fig. 4C–E). Moreover, loss of *Sod2* further exacerbated the degenerative phenotype of the RPNPC under the treatment of IL-1β, and overexpression of *Sod2* showed a robust rescuing effect against IL-1β-induced degeneration, which was confirmed by immunofluorescence staining, western blot, and apoptosis assay (Fig. 4F–O). These results demonstrate that *Sod2* deficiency accelerated IDD progression, whereas its overexpression conferred therapeutic protection against disc degeneration.

3.5. Inhibition of miR-146a-5p recovered Sod2 expression and ameliorated IDD in vivo

To investigate the therapeutic effect of miR-146a-5p inhibitor in IDD and elucidate the underlying molecular mechanisms involved, we used needle-punctured organotypic tissue-explants of rat IVD to establish an IDD model, followed by injection of miR-146a-5p mimics or inhibitors, respectively. The delivery of miR-146a-5p mimics developed an IDD phenotype, including a degradation of ECM and increased apoptosis of IVD cells, which were confirmed by immunofluorescence staining (ACAN and MMP3) and terminal deoxynucleotidyl transferase dUTP nick end labeling staining (Fig. 5A–D). Furthermore, the injection of miR-146a-5p mimics in needle-punctured IVDs further aggravated the degenerative phenotype. Conversely, local delivery of miR-146a-5p inhibitor significantly protected cultured IVDs against puncture-induced IDD phenotypes (Fig. 5A–C). Moreover, *Sod2* expression level was also detected by immunofluorescence staining, and the result showed that miR-146a-5p mimics inhibited the expression of *Sod2* and miR-146a-5p inhibitor promoted the expression of *Sod2* (Fig. 5A–E). The morphology of IVDs reflected by HE and SO staining further confirmed the protective effect of miR-146a-5p inhibitor (Fig. 5A–F). These results validated the therapeutic effect of the miR-146a-5p inhibitor in IDD and *Sod2* as a direct target of miR-146a-5p.

4. Discussion

Accumulative evidence indicates that miRNAs participate in the pathological process of IDD and modulate inflammatory responses across multiple tissues.[31] Although many miRNAs have been proved to be involved in the occurrence and development of IDD, such as miR-660,[32] miR-145,[33] and miR-34a,[34] key mediators of inflammation-induced disc degeneration remain incompletely characterized.[34,35] In this study, we first found that miR-146a-5p expression is significantly upregulated in samples acquired from severe IDD patients and IL-1β-treated cells, indicating a core role of miR-146a-5p in inflammation-induced IDD. This observed upregulation prompts consideration of the upstream drivers of miR-146a-5p expression. miR-146a-5p is a well-established inflammation-responsive miRNA, often induced via the nuclear factor Kappa-light-chain-enhancer of activated B cells (NF-κB) signaling pathway.[36,37] Pro-inflammatory cytokines like IL-1β and TNF-α, central to IDD pathogenesis,[1,2] are potent activators of NF-κB. Indeed, studies in other cell types, including chondrocytes and macrophages, have demonstrated that IL-1β/TNF-α/NF-κB signaling directly transactivates the miR146a gene.[36–38] Given the elevated levels of IL-1β and TNF-α in degenerative discs,[10] it is highly plausible that this canonical NF-κB-mediated pathway is a primary upstream regulator responsible for miR-146a-5p overexpression in our IDD patient samples and IL-1β-treated NP cells. Future research should explicitly investigate NF-κB binding to the miR146a promoter and the effects of NF-κB inhibition on miR-146a-5p levels in disc cells. Furthermore, we demonstrated that miR-146a-5p targets *Sod2* mRNA and inhibits the expression of *SOD2*, thus leading to the degradation of ECM and apoptosis of NP cells. By delineating this miR-146a-5p/*Sod2* axis, our findings establish miR-146a-5p as a critical mediator of inflammation-induced IDD pathogenesis, revealing a promising therapeutic target for disc degeneration intervention.

SODs constitute a critical class of antioxidant enzymes that neutralize reactive oxygen species (ROS) generated under cellular stress. *SOD2* is one of the most important members, which is located within the mitochondrial

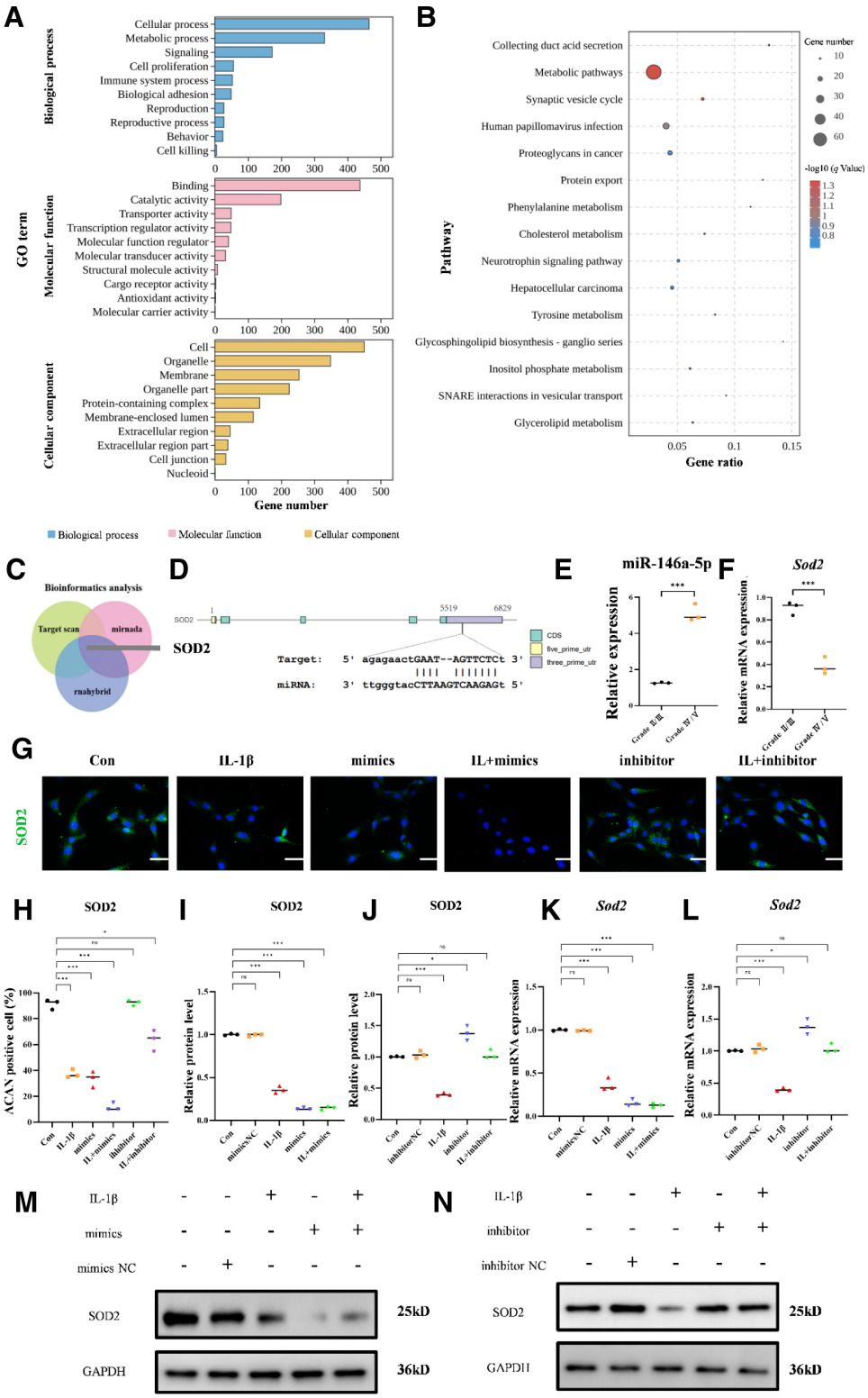

Figure 3. miR-146a-5p promoted the development of IDD by targeting *Sod2*. (A) GO enrichment analysis of genes downregulated by miR-146a-5p overexpression. (B) KEGG pathway enrichment analysis of genes downregulated by miR-146a-5p. (C) Venn diagram of bioinformatic predictions from RNAhybrid, miRanda, and TargetScan databases identifying *Sod2* as a common target of miR-146a-5p. (D) Predicted binding site of miR-146a-5p within the 3′-UTR of *Sod2* mRNA. (E) Upregulation of miR-146a-5p in severe human disc degeneration (Pfirrmann Grade IV/V) vs. mild degeneration (Grade II/III). (F) Downregulation of *Sod2* in severe human disc degeneration (Grade IV/V) vs. mild degeneration (Grade II/III). (G) Representative immunofluorescence images of SOD2 in nucleus pulposus cells: Con, IL-1β, miR-146a-5p mimics, IL + mimics, inhibitor, and IL + inhibitor groups. (H) Quantification of SOD2 immunofluorescence results (from Panel G). (I) Quantification of SOD2 WB results (from Panel M). (J) Quantification of SOD2 WB results (from Panel N). (K) qPCR results of *Sod2* in Con group, mimics NC group, IL-1β-treated group, mimics group, and IL + mimics group. (L) qPCR results of *Sod2* in Con group, inhibitor NC group, IL-1β-treated group, inhibitor group, and IL + inhibitor group. (M) WB results of SOD2 in Con group, *(Continued)*

Fig. 3 Continued. mimics NC group, IL-1β-treated group, mimics group, and IL + mimics group. (N) WB results of SOD2 in Con group, inhibitor NC group, IL-1β-treated group, inhibitor group, and IL + inhibitor group. Results were shown as mean ± S.D.; $n = 3$; * $p < 0.05$; ** $p < 0.01$; *** $p < 0.005$; ns: not statistically significant; Scale bar = 50 μm. GO = Gene Ontology; IL-1β = interleukin-1 beta; KEGG = Kyoto Encyclopedia of Genes and Genomes; SOD = superoxide dismutase; WB = western blot.

matrix, the main site of free radical production from the electron transport chain.[39] *SOD2* catalyzes the reaction of superoxide (O_2^-) to the less reactive hydrogen peroxide (H_2O_2) (which is not considered a free radical) at diffusion-limited rates, before it can oxidize macromolecules such as DNA, proteins, or lipids.[39–41] This conversion to hydrogen peroxide also facilitates a passive diffusion of hydrogen peroxide away from the mitochondrial matrix, preventing a high accumulation of superoxide close to the site of ATP production.[41,42] In this study, the bioinformatic analysis revealed that miR-146a-5p targeted the 3′-UTR of *Sod2*, and the KEGG enrichment results showed that the oxidative stress pathway was significantly enriched in the IL-1β-treated RPNPC. This finding aligns with established *SOD2* biology. Domingues CC demonstrated that overexpression of *Sod2* within human adipose-derived mesenchymal stem cells could significantly reduce oxidative stress and showed a considerable therapeutic effect on systemic inflammation.[33,41–43] Our findings resonate with recent work highlighting oxidative stress as a key driver of IDD.[44] A recent study has also established a causative link between *Sod2, Cat,* and oxidative stress in the disc, as SOD enzymes can promote the dismutation of superoxide to produce hydrogen peroxide (H_2O_2), which will be converted to water and oxygen by Catalase.[40] There were also studies that showed that SIRT3 primarily regulated mROS clearance by altering the acetylation of *SOD2*.[45] More importantly, SIRT3 directly binds and deacetylates *SOD2*, which increases *SOD2* activity and leads to a significant effect on mROS homeostasis and autophagic flux.[46,47] The identification of miR-146a-5p as a direct negative regulator of *SOD2* in NP cells adds a novel layer of post-transcriptional control to the established importance of mitochondrial antioxidant defense in disc health.[48] This mechanism parallels findings in osteoarthritis where miR-146a-5p contributes to chondrocyte dysfunction under inflammatory stress,[49] underscoring a potential common pathogenic miRNA pathway in joint and disc degeneration involving impaired antioxidant responses.

While miR-146a-5p's role in IDD remained undefined, this study employed an integrated approach: *in vitro* modeling followed by comprehensive miRNA sequencing to characterize dysregulated miRNAs in disc degeneration. Previous studies showed that, compared with the control group, miR-146a-5p in osteoarthritis samples was significantly upregulated. Some studies have also shown that miR-146a-5p promotes chondrocyte apoptosis induced by IL-1β through the TRAF6-mediated NF-κB signal pathway.[50]However, the role of miR-146a-5p in IDD was unexplored. In our study, it was found that the expression of miR-146a-5p was upregulated in degenerative RPNPC, which was consistent with the results of miRNA sequencing of RPNPC induced by inflammation, suggesting that miR-146a-5p played a key role in IDD. Therefore, we further instigated the detailed mechanism by which miR-146a-5p regulates the function and fate of RPNPC under an *in vitro* IDD model.

To explore the regulation of miR-146a-5p NPC, we used qRT-PCR to detect the effects of overexpression and silencing of miR-146a-5p on anabolism and catabolism. Overexpression of miR-146a-5p significantly decreased the production of ACAN and increased the production of MMP3 in RPNPC induced by inflammatory cytokine IL-1β. Inhibition of miR-146a-5p yielded an opposite result. After overexpression and silencing of miR-146a-5p, apoptosis was detected by flow cytometry. The results show that miR-146a-5p significantly promoted the apoptosis of RPNPC under inflammatory conditions. Subsequent mechanistic investigation identified miR-146a-5p targeted oxidative stress-related molecule *Sod2* during the development and progression of IDD. Critically, silencing of miR-146a-5p attenuated the dysfunction of RPNPC induced by inflammation *in vitro* and puncture-induced degeneration of rat NP tissue in organic tissue-explant culture.

In a word, this study established for the first time that miR-146a-5p is significantly upregulated in IDD. The presence of miR-146a-5p in RPNPC led to a decrease in the expression of its target gene *Sod2*, which in turn resulted in an increase of cell catabolism, a decrease of anabolism, an increase of apoptosis, and a degradation of ECM. Inhibition of miR-146a-5p or overexpression of *Sod2* successfully ameliorated the progression of disc degeneration (Fig. 6). These findings position the miR-146a-5p/*SOD2* axis as a crucial link between inflammation, oxidative stress, and NP cell dysfunction in IDD, offering a novel and mechanistically defined therapeutic target.

5. Conclusion

This study extends the relationship between miRNA and IVD homeostasis and provides a potential therapeutic method for the prevention and recovery of IDD by targeting miR-146a-5p.

Acknowledgements

Not applicable.

Ethics Statement

The studies involving human participants were reviewed and approved by the Institutional Review Board of Xijing Hospital of Fourth Military Medical

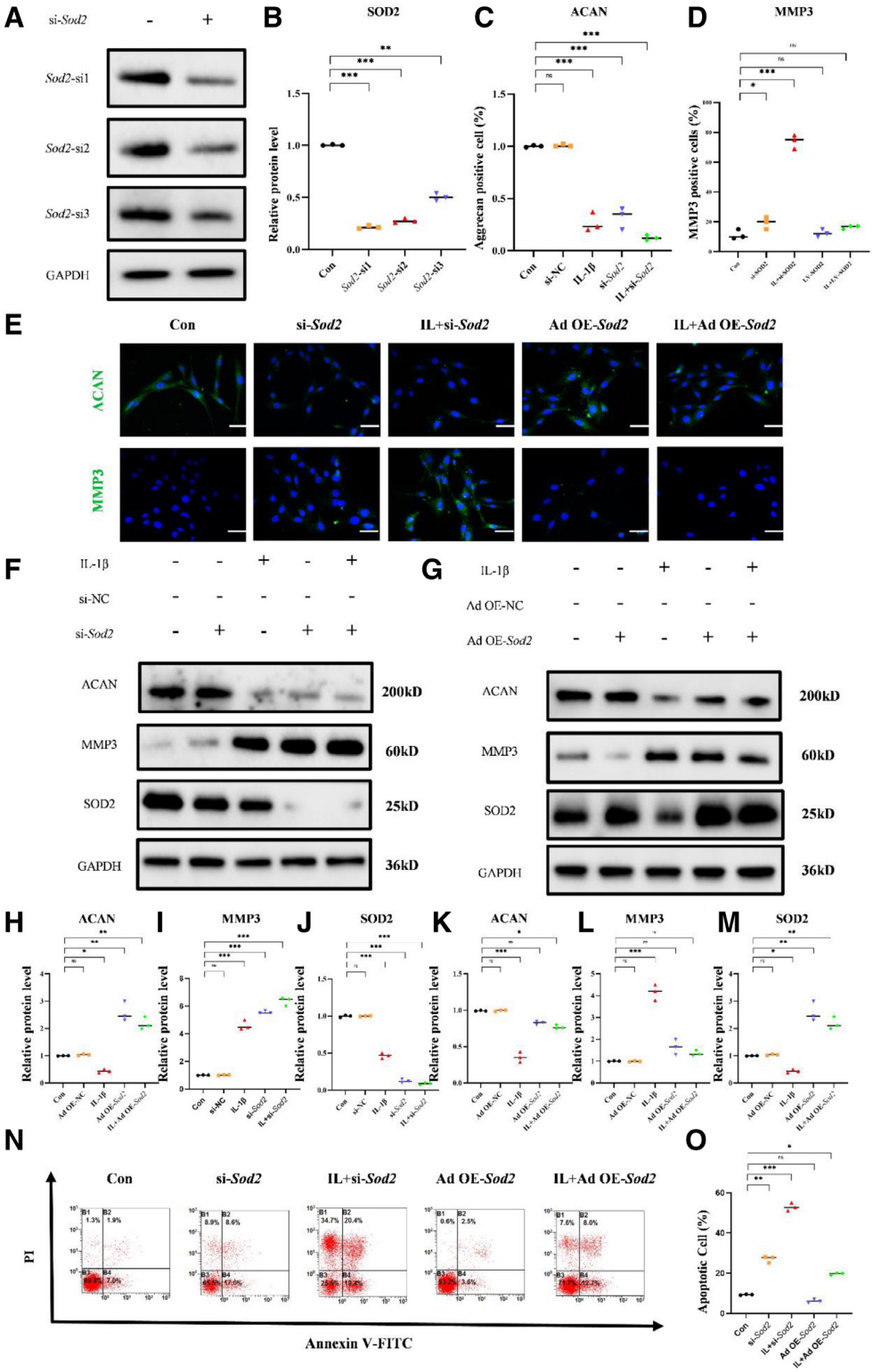

Figure 4. Loss of *Sod2* led to the development of IDD, and overexpression of *Sod2* showed a therapeutic effect *in vitro*. (A) WB results of Sod2 knockdown by 3 different siRNAs. (B) Quantification of WB results for Sod2 knockdown by 3 different siRNAs. (C) Quantification of ACAN immunofluorescence results (from Panel E). (D) Quantification of MMP3 immunofluorescence results (from Panel E). (E) Immunofluorescence images of ACAN and MMP3 in Con, si-*Sod2*, IL + si-*Sod2*, Ad OE-*Sod2*, and IL + Ad OE-*Sod2* groups. (F) WB results of ACAN, MMP3, and SOD2 in Con, si-NC, IL-1β, si-*Sod2*, and IL + si-*Sod2* groups. (G) WB results of ACAN, MMP3, and SOD2 in Con, Ad OE-NC, IL-1β, Ad OE-*Sod2*, and IL + Ad OE-*Sod2* groups. (H) Quantification of ACAN WB results (from Panel F). (I) Quantification of MMP13 WB results (from Panel F). (J) Quantification of SOD2 WB results (from Panel F). (K) Quantification of ACAN WB results (from Panel G). (L) Quantification of MMP13 WB results (from Panel G). (M) Quantification of SOD2 WB results (from Panel G). (N) Apoptosis flow cytometry results in Con, si-*Sod2*, IL + si-*Sod2*, Ad OE-*Sod2*, and IL + Ad OE-*Sod2* groups. (O) Quantification of apoptosis flow cytometry results. Results were shown as mean ± S.D.; n = 3; *$p < 0.05$; **$p < 0.01$; ***$p < 0.005$; ns: not statistically significant; Scale bar = 50 μm. IDD = intervertebral disc degeneration; ACAN = aggrecan; IL-1β = interleukin-1 beta; MMP3 = matrix metalloproteinase 3; SOD = superoxide dismutase; WB = western blot.

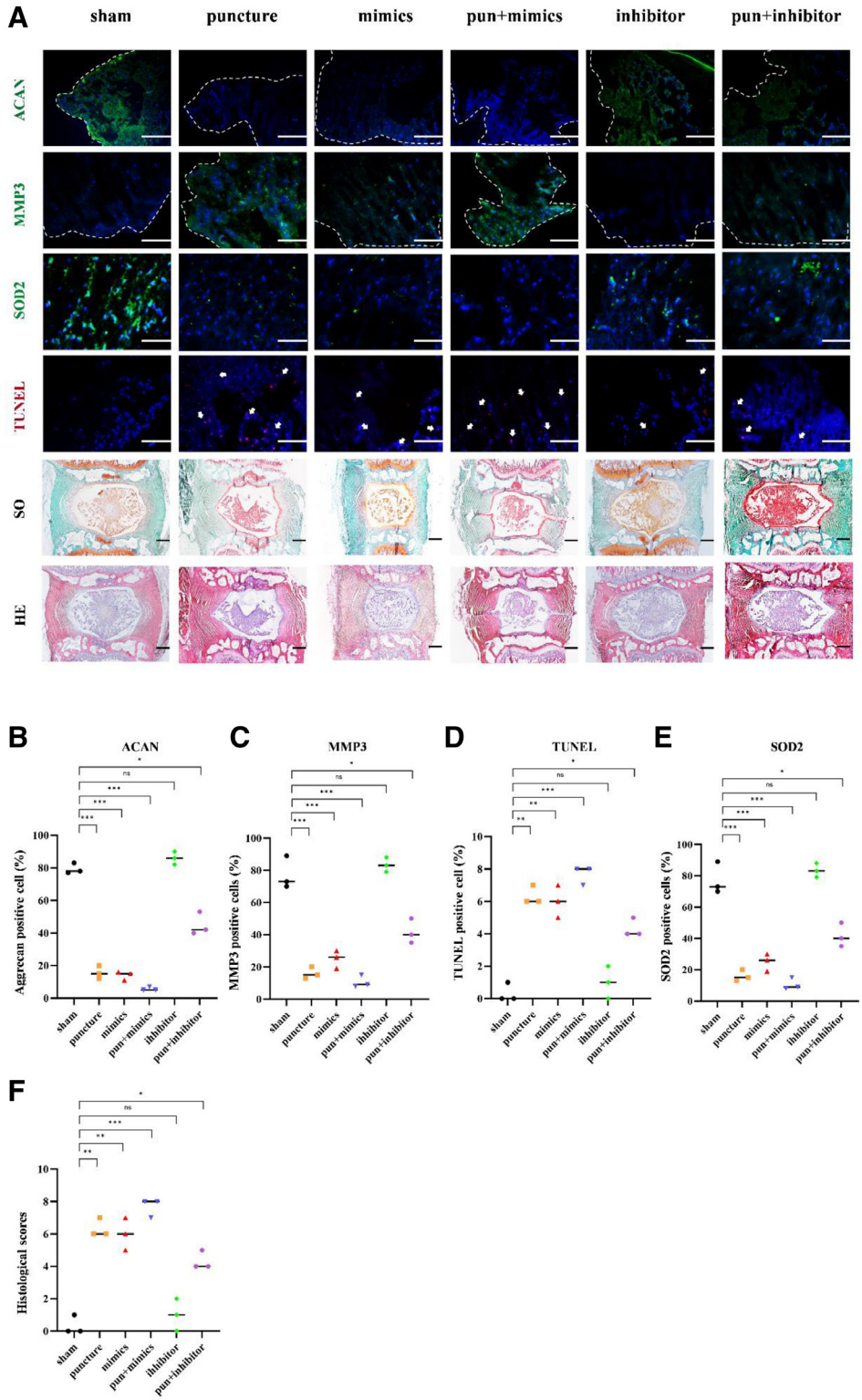

Figure 5. Inhibition of miR-146a-5p ameliorated IDD in vivo. (A) ACAN, MMP3, SOD immunofluorescence staining, TUNEL staining, and SO/HE histological staining in Sham, puncture, mimics, pun + mimics, inhibitor, and pun + inhibitor groups. (B) Quantification of ACAN immunofluorescence staining. (C) Quantification of MMP3 immunofluorescence staining. (D) Quantification of TUNEL staining. (E) Quantification of SOD immunofluorescence staining. (F) Histological score. Results were shown as mean ± S.D.; $n = 3$; $^{*}p < 0.05$; $^{**}p < 0.01$; $^{***}p < 0.005$; ns: not statistically significant; Scale bar = 20 μm (IF staining); Scale bar = 500 μm (histology staining). The white arrow indicates TUNEL-positive cells. ACAN = aggrecan; IDD = intervertebral disc degeneration; MMP3 = matrix metalloproteinase 3; SOD = superoxide dismutase; TUNEL = terminal deoxynucleotidyl transferase dUTP nick end labeling.

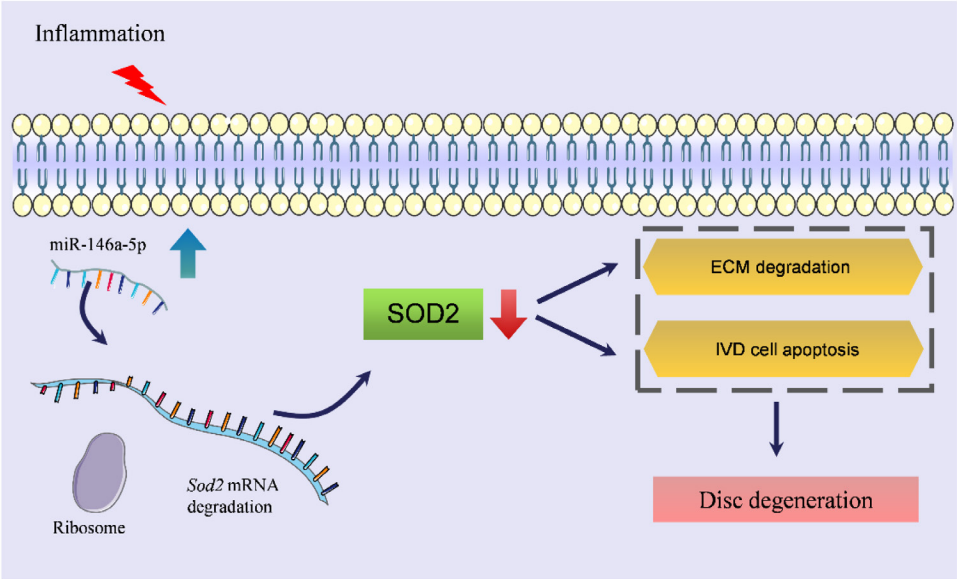

Figure 6. Schematic diagram summarizing the pathogenic role of miR-146a-5p in RPNPCs: By directly targeting and suppressing *Sod2* expression, miR-146a-5p overexpression promotes cellular catabolism, inhibits anabolic processes, induces apoptosis, and accelerates extracellular matrix (ECM) degradation, collectively driving intervertebral disc degeneration. RPNPCs = rat primary nucleus pulposus cells; SOD = superoxide dismutase.

University. The patients/participants provided their written informed consent to participate in this study. The animal study was reviewed and approved by the Animal Use and Care Committee of the Fourth Military Medical University.

Conflicts of interest

The authors have no conflicts of interest to disclose.

Funding source

This work was supported by the National Natural Science Foundation of China (82020108019, 82394442, 82402847, 82302742, 82430077), Shaanxi Province Health Commission Bone and Joint Degeneration, Regeneration and Injury Reconstruction Research and Innovation Team (2025TD-14), and Young Talent Fund of Association for Science and Technology in Shaanxi, China (20250317).

Data availability statement

Data collected and analyzed for the study are available from the corresponding authors upon reasonable request.

Author contributions

Designed the experiments: Dong Wang, Liu Yang, Zhuojing Luo.

Carried out most of the experiments: Dong Wang, Chu Gao.

All authors analyzed the data, wrote the manuscript, and approved the final manuscript.

References

[1] Chen S, Chen M, Wu X, et al. Global, regional and national burden of low back pain 1990-2019: a systematic analysis of the Global Burden of Disease study 2019. J Orthop Translat. 2022;32:49–58.

[2] Patrick N, Emanski E, Knaub MA. Acute and chronic low back pain. Med Clin North Am. 2014;98:777–89, xii.

[3] Clouet J, Vinatier C, Merceron C, et al. The intervertebral disc: from pathophysiology to tissue engineering. Joint Bone Spine. 2009;76:614–8.

[4] Hoy D, March L, Brooks P, et al. The global burden of low back pain: estimates from the Global Burden of Disease 2010 study. Ann Rheum Dis. 2014;73:968–74.

[5] Mokdad AH, Ballestros K, Echko M, et al; US Burden of Disease Collaborators. The State of US Health, 1990-2016: burden of diseases, injuries, and risk factors among US states. JAMA. 2018;319:1444–72.

[6] Gianola S, Bargeri S, Del Castillo G, et al. Effectiveness of treatments for acute and subacute mechanical non-specific low back pain: a systematic review with network meta-analysis. Br J Sports Med. 2022;56:41–50.

[7] Knezevic NN, Candido KD, Vlaeyen JWS, Van Zundert J, Cohen SP. Low back pain. Lancet. 2021;398:78–92.

[8] Choi H, Tessier S, Silagi ES, et al. A novel mouse model of intervertebral disc degeneration shows altered cell fate and matrix homeostasis. Matrix Biol. 2018;70:102–22.

[9] Global Burden of Disease Study 2013 Collaborators. Global, regional, and national incidence, prevalence, and years lived with disability for 301 acute and chronic diseases and injuries in 188 countries, 1990-2013: a systematic analysis for the Global Burden of Disease Study 2013. Lancet. 2015;386:743–800.

[10] Risbud MV, Shapiro IM. Role of cytokines in intervertebral disc degeneration: pain and disc content. Nat Rev Rheumatol. 2014;10:44–56.

[11] Ghannam M, Jumah F, Mansour S, et al. Surgical anatomy, radiological features, and molecular biology of the lumbar intervertebral discs. Clin Anat. 2017;30:251–66.

[12] Bian Q, Ma L, Jain A, et al. Mechanosignaling activation of TGFbeta maintains intervertebral disc homeostasis. Bone Res. 2017;5:17008.
[13] Chen S, Wu X, Lai Y, et al. Kindlin-2 inhibits Nlrp3 inflammasome activation in nucleus pulposus to maintain homeostasis of the intervertebral disc. Bone Res. 2022;10:5.
[14] Francisco V, Pino J, Gonzalez-Gay MA, et al. A new immunometabolic perspective of intervertebral disc degeneration. Nat Rev Rheumatol. 2022;18:47–60.
[15] Peng P, Wang D, Xu X, et al. Targeting clock-controlled gene Nrf2 ameliorates inflammation-induced intervertebral disc degeneration. Arthritis Res Ther. 2022;24:181.
[16] Phillips KL, Jordan-Mahy N, Nicklin MJ, Le Maitre CL. Interleukin-1 receptor antagonist deficient mice provide insights into pathogenesis of human intervertebral disc degeneration. Ann Rheum Dis. 2013;72:1860–7.
[17] Han B, Zhu K, Li FC, et al. A simple disc degeneration model induced by percutaneous needle puncture in the rat tail. Spine (Phila Pa 1976). 2008;33:1925–34.
[18] Lu TX, Rothenberg ME. MicroRNA. J Allergy Clin Immunol. 2018;141:1202–7.
[19] Cazzanelli P, Wuertz-Kozak K. MicroRNAs in intervertebral disc degeneration, apoptosis, inflammation, and mechanobiology. Int J Mol Sci. 2020;21(10):3601.
[20] Ji ML, Jiang H, Zhang XJ, et al. Preclinical development of a microRNA-based therapy for intervertebral disc degeneration. Nat Commun. 2018;9:5051.
[21] Jiang H, Moro A, Wang J, Meng D, Zhan X, Wei Q. MicroRNA-338-3p as a novel therapeutic target for intervertebral disc degeneration. Exp Mol Med. 2021;53:1356–65.
[22] Chen Z, Liao Z, Liu M, et al. Nucleus pulposus-targeting nanocarriers facilitate mirna-based therapeutics for intervertebral disc degeneration. Adv Healthc Mater. 2023;12:e2301337.
[23] Mei L, Zheng Y, Gao X, et al. Hsa-let-7f-1-3p targeting the circadian gene Bmal1 mediates intervertebral disc degeneration by regulating autophagy. Pharmacol Res. 2022;186:106537.
[24] Krol J, Loedige I, Filipowicz W. The widespread regulation of microRNA biogenesis, function and decay. Nat Rev Genet. 2010;11:597–610.
[25] Li J, Zhang Y, Fu T, Xing G, Tong Y. Advancing cancer therapy: the role of MicroRNA in clinical applications. Pharmacol Res. 2024;206:107299.
[26] Wang D, Peng P, Dudek M, et al. Restoring the dampened expression of the core clock molecule BMAL1 protects against compression-induced intervertebral disc degeneration. Bone Res. 2022;10:20.
[27] Wang D, Zhang P, Xu X, et al. Knockdown of cytokeratin 8 overcomes chemoresistance of chordoma cells by aggravating endoplasmic reticulum stress through PERK/eIF2α arm of unfolded protein response and blocking autophagy. Cell Death Dis. 2019;10:887.
[28] Wang D, Shang Q, Mao J, et al. Phosphorylation of KRT8 (keratin 8) by excessive mechanical load-activated PKN (protein kinase N) impairs autophagosome initiation and contributes to disc degeneration. Autophagy. 2023;19:2485–503.
[29] Mao J, Wang D, Wang D, et al. SIRT5-related desuccinylation modification of AIFM1 protects against compression-induced intervertebral disc degeneration by regulating mitochondrial homeostasis. Exp Mol Med. 2023;55:253–68.
[30] Shang Q, Wang D, Wang D, et al. Facet joint degeneration—An initial procedure of the cervical spine degeneration. JOR Spine. 2023;6:e1241.
[31] Lan T, Shiyu H, Shen Z, Yan B, Chen J. New insights into the interplay between miRNAs and autophagy in the aging of intervertebral discs. Ageing Res Rev. 2021;65:101227.
[32] Zhang HJ, Ma XH, Xie SL, Qin SL, Liu CZ, Zhang ZG. Knockdown of miR-660 protects nucleus pulposus cells from TNF-a-induced apoptosis by targeting serum amyloid A1. J Orthop Surg Res. 2020;15:7.
[33] Zhou J, Sun J, Markova DZ, et al. MicroRNA-145 overexpression attenuates apoptosis and increases matrix synthesis in nucleus pulposus cells. Life Sci. 2019;221:274–83.
[34] Chen H, Wang J, Hu B, et al. MiR-34a promotes Fas-mediated cartilage endplate chondrocyte apoptosis by targeting Bcl-2. Mol Cell Biochem. 2015;406:21–30.
[35] Li X, An Y, Wang Q, Han X. The new ceRNA crosstalk between mRNAs and miRNAs in intervertebral disc degeneration. Front Cell Dev Biol. 2022;10:1083983.
[36] Taganov KD, Boldin MP, Chang KJ, Baltimore D. NF-kappaB-dependent induction of microRNA miR-146, an inhibitor targeted to signaling proteins of innate immune responses. Proc Natl Acad Sci U S A. 2006;103:12481–6.
[37] Perry MM, Moschos SA, Williams AE, Shepherd NJ, Larner-Svensson HM, Lindsay MA. Rapid changes in microRNA-146a expression negatively regulate the IL-1beta-induced inflammatory response in human lung alveolar epithelial cells. J Immunol. 2008;180:5689–98.
[38] Pauley KM, Satoh M, Chan AL, Bubb MR, Reeves WH, Chan EK. Upregulated miR-146a expression in peripheral blood mononuclear cells from rheumatoid arthritis patients. Arthritis Res Ther. 2008;10:R101.
[39] Flynn JM, Melov S. SOD2 in mitochondrial dysfunction and neurodegeneration. Free Radic Biol Med. 2013;62:4–12.
[40] Xiao L, Xu SJ, Liu C, Wang J, Hu B, Xu HG. Sod2 and catalase improve pathological conditions of intervertebral disc degeneration by modifying human adipose-derived mesenchymal stem cells. Life Sci. 2021;267:118929.
[41] Murphy MP. How mitochondria produce reactive oxygen species. Biochem J. 2009;417:1–13.
[42] Daly MJ. Death by protein damage in irradiated cells. DNA Repair (Amst). 2012;11:12–21.
[43] Shen J, Zhu X, Liu H. MiR-483 induces senescence of human adipose-derived mesenchymal stem cells through IGF1 inhibition. Aging (Albany NY). 2020;12:15756–70.
[44] Dimozi A, Mavrogonatou E, Sklirou A, Kletsas D. Oxidative stress inhibits the proliferation, induces premature senescence and promotes a catabolic phenotype in human nucleus pulposus intervertebral disc cells. Eur Cell Mater. 2015;30:89–102; discussion 103.
[45] Qu ZA, Ma XJ, Huang SB, et al. SIRT2 inhibits oxidative stress and inflammatory response in diabetic osteoarthritis. Eur Rev Med Pharmacol Sci. 2020;24:2855–64.
[46] Dikalova AE, Itani HA, Nazarewicz RR, et al. Sirt3 impairment and SOD2 hyperacetylation in vascular oxidative stress and hypertension. Circ Res. 2017;121:564–74.
[47] Zhang H, Ma Y, Wang M, Elsabagh M, Loor JJ, Wang H. Dietary supplementation of l-arginine and N-carbamylglutamate enhances duodenal barrier and mitochondrial functions and suppresses duodenal inflammation and mitophagy in suckling lambs suffering from intrauterine-growth-restriction. Food Funct. 2020;11:4456–70.
[48] Yamasaki K, Nakasa T, Miyaki S, et al. Expression of MicroRNA-146a in osteoarthritis cartilage. Arthritis Rheum. 2009;60:1035–41.
[49] Li J, Huang J, Dai L, et al. miR-146a, an IL-1β responsive miRNA, induces vascular endothelial growth factor and chondrocyte apoptosis by targeting Smad4. Arthritis Res Ther. 2012;14:R75.
[50] Shao J, Ding Z, Peng J, et al. MiR-146a-5p promotes IL-1β-induced chondrocyte apoptosis through the TRAF6-mediated NF-kB pathway. Inflamm Res. 2020;69:619–30.